Photoacoustic zinc phthalocyanine scaffolds for augmenting PDT outcomes

INTRODUCTION

Molecular imaging for cancer therapy assessment:

Cancer is a leading cause of mortality worldwide for which a uniform treatment or diagnostic method has not sufficed. In case of localized non-metastatic cancers, surgery and radiotherapy are the two primary treatment routes, whereas chemotherapeutics hold potential for treatment of all cancer stages. To assess tumor response to therapy, Response Evaluation Criteria in Solid Tumors (RECIST) and World Health Organization (WHO) response criteria employ the changes in tumor size determined by the conventional imaging modalities such as computed tomography (CT), magnetic resonance imaging (MRI) and positron emission tomography (PET). However, depending on the tumor type and stage, tumor size might be an inaccurate parameter to justify the efficacy of treatment, thereby resulting in delayed assessment of response.[1] Photoacoustic imaging (PAI), is a relatively new molecular imaging method with great translational potential for the clinic due to its ability to provide both anatomical and functional information with excellent spatio-temporal resolution at tissue depths of 3-5 cm. The principle of PAI involves acoustic detection of optical absorption by chromophores when excited in near-infrared (NIR) range and therefore risk of radiation exposure with this modality is nil.

PAI as therapy assessment tool:

Radiology methods, especially nuclear medicine or PET imaging in combination with CT, is for noninvasive analyses of treatment responses at different stages in cancer patients. However, PET cannot be used regularly in patients due to risk of accumulated radiation dosage and use of radioactivity. Photoacoustic imaging can also evaluate treatment response with an advantageous edge over PET, since does not involve any radioactive isotope or ionizing radiation. PAI is reported to successfully guide therapies such as anti-vascular therapy by monitoring changes in haemoglobin PA signal in real-time[2], photothermal therapy (PTT)[3] and also photodynamic therapy (PDT)[4]. PDT renders light-mediated cytotoxicity by generating singlet oxygen or reactive oxygen species (ROS) through a photosensitizer (PS) moiety when irradiated by a specific wavelength of light in the NIR range. Due to the weak biodistribution of PS small molecules and low penetration of light in tissues, PDT outcomes are majorly debilitated. PAI can facilitate PDT outcomes in real-time in the following ways: (a) A PS with low fluorescence quantum yield can act as a better PA contrast agent than optical dyes currently employed.[5] For example, zinc phthalocyanines possess a 50% higher PA quantum yield compared to protoporphyrin IX, the photosensitizer and metabolic end product of 5-ALA, administered to patients in the clinic for PDT.[6]. (b) PAI can be utilized to monitor PDT-induced dose-dependent vascular damage and can also generate maps of vascular structure from deep-seated tissues.[7, 8] (c) PAI can assess the changes in oxygen saturation of the whole tumor volume induced by PDT. Therefore, photoacoustic image guided therapy can provide insights to current therapeutic mechanisms and suggest new and improved methods.

Small molecule theranostic probes for PDT and PAI

Currently, only small molecules are approved for PDT in the clinic such as Porfimer sodium (Photofrin®) – a hematoporphyrin derivative (for obstructive esophagel or lung cancer), Temoporfin (Foscan®) – a chlorin derivative (for advanced head and neck cancer)[9], and 5-aminolevulinic Acid (5-ALA) (for actinic keratosis, brain) and its methyl ester (methyl-ALA).[10] The weak biodistribution and off-target localization and mild cytotoxicity of these agents have inspired the formulation of some of these PS with liposomes or nanoparticle carriers although challenges such as instability, , complexity, and uncertain nanomaterial toxicity have impeded their clinical translation. Phthalocyanines are a class of small molecules that absorb light in the NIR wavelength and can serve as effective photosensitizers. To this effect, unsubstituted Si and Zn-phthalocyanines have been studied as PDT agents.[11, 12] They can be further tuned to incorporate various functionalities that improve solubility, enhance singlet oxygen generation efficiency with heavy atom substitution such as Br or I or to specific organelle in the cells (introducing charge).

We have developed a class of substituted Zn-phthalocyanines, incorporating 1) substitutions rich in -OH functionality at different positions -peripheral/non-peripheral of the isoindoline ring and 2) one iodo-substitution in each, to increase singlet oxygen quantum efficiency. Here, we report the chemical synthesis, and photophysical and spectroscopic characterization of these agents, along with in vitro and in vivo studies that demonstrate their promise as the next-generation theranostic agents in a set of pancreatic cancer cell lines.

OBJECTIVES

Synthesize functionalized Zn-phthalocyanines for theranostics.

(a). Chemical synthesis and characterization of probes using NMR, HPLC and mass spectrometry.

(b). Photophysical studies including absorbance, fluorescence, and photoacoustic characterization.

(c). Biochemical characterization for stability and photobleaching properties

(d). Determination of singlet oxygen quantum yields

(e). Cellular uptake and intracellular ROS generation in two human pancreatic cancer cell lines, PANC-1 and BxPC-3

(f). Dark cytotoxicity (without laser irradiation) and light cytotoxicity (with laser irradiation) of the developed probes in comparison to commercially available photosensitizer- $ZnPcS_4$ in PANC-1 and BxPC-3

(g). *In vivo* biodistribution studies with PANC-1 tumor model in the flank of mouse

(h). *Ex-vivo* studies to test the clearance of probes from the tumor and accumulation in different organs

(i). Histology studies to monitor the morphology of the organs through H and E stain after probe administration

MATERIAL AND METHODS

Chemical synthesis of the substituted ZnPc probes:

The synthesis scheme has not been disclosed as these agents are currently under the process of patent clearance.

Photophysical Properties:

UV-visible spectra were collected for wavelengths ranging from 280-900 nm using the spectrophotometer and molar extinction coefficient (ε) for each probe was determined in DMSO. Meanwhile, the fluorescence emission spectra of the probes were recorded at 650-850 nm following excitation at 435 nm using a plate reader (BioTek Synergy H1 Hybrid multimode reader). ZnPcS4 with φFstd = 0.07 (DMSO) was used as reference.

Photoacoustic imaging (PAI) studies using multispectral optoacoustic tomography (MSOT) scanner:

Tissue mimicking phantom preparation:

0.75 g of agar was added to 50 ml of Milli-Q water and heated in microwave until it boils, with gentle shaking. The solution was repeatedly heated until no remaining agar powder was visible. The agar solution was taken out of the microwave and 1.03 ml of intralipid was added and mixed gently. 20 ml syringes with their front part cut-off and an internal diameter of 2 cm were used as molds to prepare phantoms. The solution was poured into the plastic syringes. Two straws having a diameter of 3 mm were immediately placed into the syringe and held in position using the phantom caster provided with the phantom kit. The solution was cooled at 4 °C for 30 minutes. The phantoms were immersed in Milli-Q water, stored at 4 °C in the fridge and used for PAI.

Photoacoustic imaging:

A preclinical multi-spectral optoacoustic tomography (MSOT) scanner (MSOT inVision 256, iThera Medical, Munich, Germany) was used for all photoacoustic imaging studies. Data acquisition was performed in the wavelength range of 680–900 nm in 2 nm steps, using 10 averages frames per wavelength. The fibre bundle and the transducer array are stationary, while the sample holder moves along the z-direction allowing longitudinal acquisition of different imaging planes using a moving stage. MSOT measurements were performed in a temperature-controlled water bath at 36 °C.

PA absorbance study:

To compare the photoacoustic signal of the synthesized probes, 50 μM concentrations of each were prepared in DMSO, PBS and PBS+2% Triton-X 100. Solutions were filled in capillaries sealed from both ends and placed at the centre of the imaging phantom. Samples were imaged using the parameters and method mentioned above.

Biochemical stability study:

Mouse serum was used to test the time-dependent stability of the synthesized probes. 50 μM concentrations of each probe were prepared in mouse serum. Solutions were filled in capillaries sealed from both ends and placed at the centre of the imaging phantom. Samples

were imaged using the parameters and method mentioned above. Scans were acquired at time points of 0, 0.5, 1, 1.5, 2, 3, 4, 5, 6, 8, and 12 hours.

Photostability study:

The photobleaching effect associated with the synthesized probes was studied by testing their photostability in mouse serum. 50 μM concentrations of each probe were prepared in mouse serum. Solutions were filled in capillaries sealed from both ends and placed at the centre of the imaging phantom. The laser wavelength was set to 700 nm to obtain maximum signal, pulsed with 50 averages for an image every 30 seconds and continuously repeated for 30 minutes. The data acquired was used to plot signal vs. time to check photostability.

Measurement of the singlet oxygen generation:

Singlet oxygen generation efficiency was estimated according to the literature. Methylene blue was used as a reference and DPBF was used as an oxygen quencher. The initial absorbance of DPBF was adjusted to about 1.0 in DMSO. Then, the photosensitizer was added to the cuvette and photosensitizer's absorbance was adjusted to about 0.1-0.3. The photooxidation of DPBF was monitored between 0-300 s depending on the efficiency of the photosensitizer. DPBF absorbance was plotted as a function of irradiation time.

Cellular uptake and intracellular ROS production:

BxPC-3 and PANC-1 cells were seeded in 35-mm dishes. 1 μM of α-ZnPc, 10 μM of β-ZnPc and 20 μM of ZnPcS4 photosensitizers were added to 8 dishes each and incubated for 15 minutes, 2 hours, 4 hours and 6 hours at 37 ℃ in a 5% CO_2 incubator. The cells were washed twice with PBS and incubated with DHR123 for 15 minutes. Out of 8 dishes per agent, 4 were kept under the dark conditions (control) and 4 were irradiated with a 740 nm lamp for 2 minutes at 100 mW/cm^2. The cellular uptake and intracellular ROS generation as recorded by flow cytometer.

Cell Culture:

Pancreatic cancer cell lines PANC-1 (human) and BxPC-3 (human) were obtained from ATCC. PANC-1 cells were cultured in DMEM media (Lonza) and BxPC-3 cells were maintained in RPMI 1640 (Lonza) supplemented with 10% FBS (Gibco) and 1% Penicillin-streptomycin antibiotic (Lonza). Cells were grown at 37 ℃ in a 5% CO_2 incubator.

Cytotoxicity – Dark and light:

BxPC-3 and PANC-1 were seeded in 96-well plates with a density of 15000 cells per well and allowed to grow for 24 hours. $ZnPcS_4$ and the synthesized probes were added in the concentration range of 1-100 μM in triplicates and incubated for 4 hours. The cells were fixed with 30% trichloroacetic acid, washed and air dried. Sulforhodamine B (SRB) assay was performed to estimate the cell viability.

Animal model:

All animal experimental procedures were performed in accordance with the protocol #977/2023 approved by the Institutional Animal Ethics Committee (IAEC). Xenograft mice models were established by injecting subcutaneously into the right flank of mouse, 0.2 mL of cell suspension containing 5x10^6 PANC-1, a human pancreatic cancer cell line and matrigel

(BD biosciences) in 1:1 volume ratio. When the tumor volume reached a palpable size, the mouse was used for in vivo PA imaging.

***In vivo* longitudinal monitoring of probe biodistribution in mouse xenograft model:**

ZnPc at a dosage of 0.42 mg/kg was injected through the tail vein of tumor-bearing mice anaesthetized under isoflurane (2.5-3%) and the probe biodistribution was monitored over time in various organs using PA imaging. Before image acquisition, a volume ROI consisting of transverse slices with a step size of 0.5 mm spanning from the liver to the lower abdomen was selected by manual inspection of live MSOT images, and the 8 laser excitation wavelengths of 680, 700, 720, 740, 760, 780, 800, and 820 nm were selected for correspondence with the absorption spectra of α-ZnPc, β-ZnPc, oxy- and deoxy-haemoglobin. Multispectral imaging was then performed with 10 signal averages per wavelength per transverse slice, at 45 min, 3, 6, and 12 hr postinjection.

Image reconstruction and multispectral processing.

Images were reconstructed using a back-projection based approach for offline analysis. After image reconstruction, spectral unmixing was performed to resolve individual components from different chromophores in the system. For each pixel in the image, the method fits the total measured optoacoustic spectrum to the known absorption spectra of the individual chromophores, based on least-squares linear regression.

***Ex vivo* photoacoustic imaging and quantification of PA signal intensity in major organs:**

To further validate the biodistribution of α-ZnPc and β-ZnPc, the major organs (heart, liver, kidney, spleen, and tumor) were collected, and the PA intensity was detected using the MSOT scanner.

Histological examination of PANC-1 tumor mouse model:

Liver and kidney were collected and fixated with 4% paraformaldehyde. The fixed organs slices were sent to RV Diagnostics lab for hematoxylin and eosin staining. The histological images were taken using a bright-field microscope.

RESULTS AND DISCUSSION

Purification and validation of the agents

In the 3-step synthesis scheme, the products of the intermediate steps were validated with 1H and 13C NMR and HRMS. The final product purity was assessed with HPLC followed by MALDI mass spectrometry. ZnPc 6a (α-ZnPc) [M+H]: 973.1 and ZnPc 6b **(**β-ZnPc) [M+H]: 973.1 **(Figure 1 a-f)**

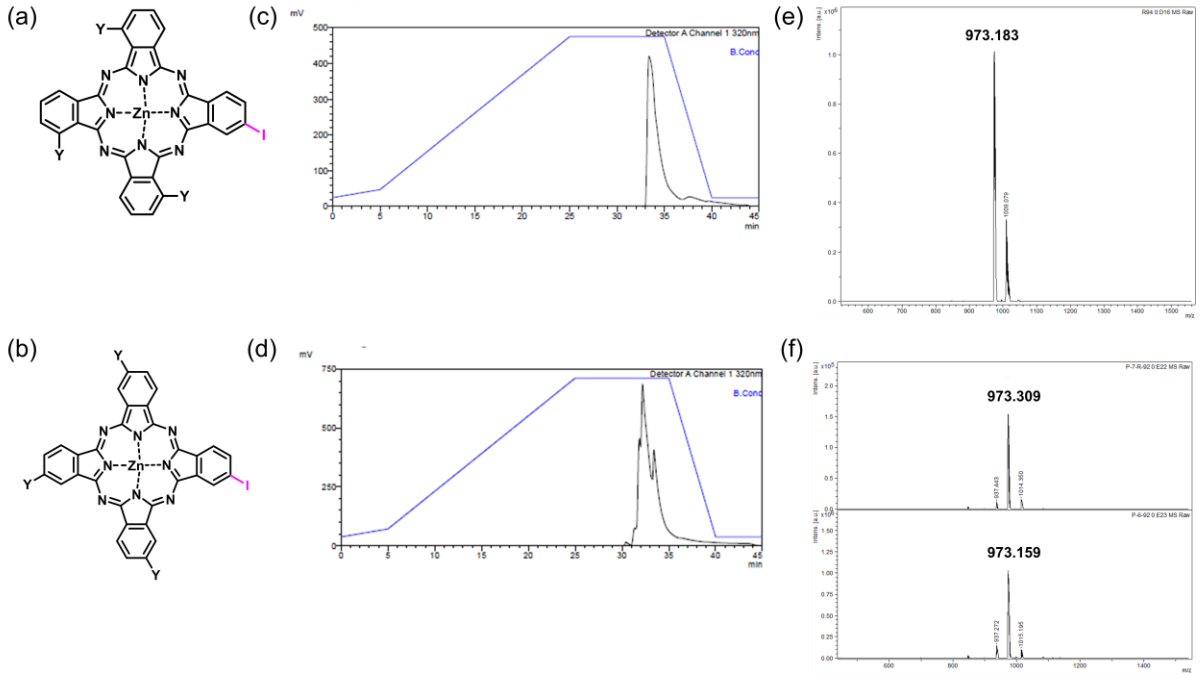

Figure 1: Chemical structures of **(a)** α-ZnPc and **(b)** β-ZnPc; HPLC chromatograms of **(c)** α-ZnPc and **(d)** β-ZnPc; MALDI-TOF mass spectra of **(e)** α-ZnPc and **(f)** β-ZnPc

Photoacoustic agents, α-ZnPc and β-ZnPc, absorb in the NIR window, exhibit low fluorescence quantum yields and high molar extinction coefficients

The proposed agents α-ZnPc and β-ZnPc have an absorbance maximum in the range of 680-700 nm **(Figure 2 a,b)**. α-ZnPc which has the substitutions at the non-peripheral alpha position of the isoindoline ring has a slightly red-shifted NIR absorbance at 698 nm as compared to the β-ZnPc with same substitutions at the peripheral beta position. α-ZnPc also exhibited 3-fold higher molar absorption coefficient (Ɛ) as compared to β-ZnPc **(Figure 2 c)**. The agents possess similar fluorescence emission wavelength in the range of 690-710 nm **(Figure 2 d)** with relatively low fluorescence quantum yields (φ_F) in DMSO ranging from 0.03 to 0.06 **(Figure 2 e)** as calculated by using $ZnPcS_4$ (φ_F = 0.07 in DMSO) as a reference. Same substitutions at different positions in α-ZnPc and β-ZnPc lowered the fluorescence quantum yields of these phthalocyanines regardless of the common iodo-substitution suggesting a higher photoacoustic efficiency.

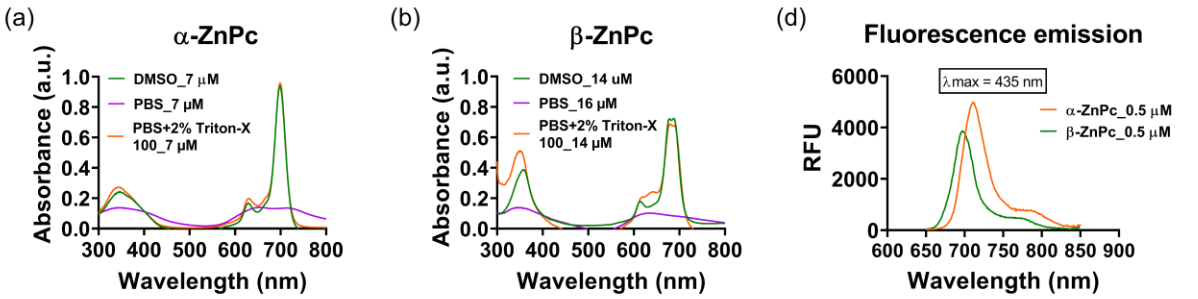

(c)

Photosensitizer	DMSO		PBS		PBS + 2% Triton-X 100	
	λmax (nm)	ε ($M^{-1}cm^{-1}$)	λmax (nm)	ε ($M^{-1}cm^{-1}$)	λmax (nm)	ε ($M^{-1}cm^{-1}$)
α-ZnPc	698.5	174469	655	19048	699	143037
β-ZnPc	687.5	50552	634	9749	679	49999

(e)

Photosensitizer	DMSO (φ_F)
α-ZnPc	**0.03**
β-ZnPc	**0.06**
$ZnPcS_4$	0.07

Figure 2: Absorbance spectra of **(a)** α-ZnPc and **(b)** β-ZnPc in DMSO, PBS, and PBS+2% Triton-X 100; **(c)** Absorbance maxima and molar extinction coefficients of α-ZnPc and β-ZnPc in DMSO, PBS, and PBS+2% Triton-X 100; **(d)** Fluorescence emission spectra of α-ZnPc and β-ZnPc in DMSO; **(e)** Fluorescence quantum yields (φ_F) of α-ZnPc and β-ZnPc in relation to $ZnPcS_4$.

Agents have good biochemical stability and minimal photobleaching with α-ZnPc having a higher PA intensity

When tested for biochemical stability in mouse serum, α-ZnPc and β-ZnPc, were found to be stable with minimal variations in the PA signal intensity from 0 to 12 hours **(Figure 3 a)**. *In vivo* studies with these probes would be conducted in a time frame of 8 h post-injection and our results suggest that these probes are stable over time for such studies.

When tested for photostability in mouse serum to study the photobleaching effect, α-ZnPc and β-ZnPc, showed a stable PA signal intensity over multiple scans acquired for a period of 25 minutes with continuous laser irradiation at the λ_{max} of respective probes **(Figure 3 b)**. The results suggest that our probes have minimal photobleaching effect signifying their suitability for both *in vivo* studies and future clinical translation.

At wavelengths beyond 900 nm, absorption of water increases significantly, making the 660-900 nm window optimal for *in vivo* deep tissue imaging. Fluorescence quantum yields of all the phthalocyanine scaffolds generated are lower than the optical dyes ICG and IRDye800, which are employed in the clinic as optical agents. Lower fluorescence quantum yields suggest higher photoacoustic quantum yields. The photoacoustic spectra acquired for these agents depict that α-ZnPc has a 2-fold higher photoacoustic signal intensity attributed to its lower fluorescence quantum yield and higher molar absorption coefficient **(Figure 3 c,d)**.The above-mentioned characteristics of both the agents make them potent photoacoustic contrast agent for imaging deep-seated tissues.

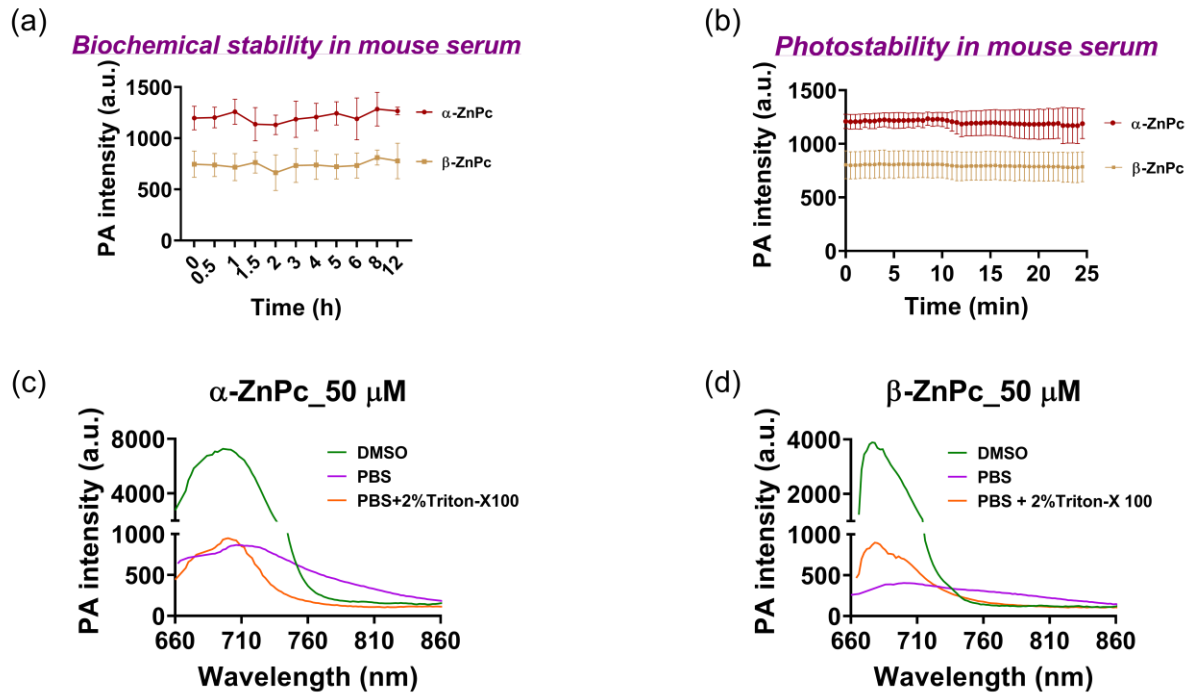

Figure 3: Stability studies of α-ZnPc and β-ZnPc in mouse serum: **(a)** Biochemical stability and **(b)** Photostability; Photoacoustic spectra in DMSO, PBS, and PBS + 2% Triton-X 100: **(c)** α-ZnPc and **(d)** β-ZnPc.

Substitution at non-peripheral alpha position of the isoindoline ring shows higher singlet oxygen generation efficiency

The singlet oxygen generation efficiency was estimated using methylene blue as a reference. The efficiency was compared with the commercially available $ZnPcS_4$. Since the singlet oxygen generation efficiency for both the agents, α-ZnPc and β-ZnPc, is higher than $ZnPcS_4$, it indicates that the incorporation of -iodo substitution generates a long-lived triplet state which enhances the production of singlet oxygen species. Interestingly, keeping the -iodo substitution same, substitutions at non-peripheral alpha position boosts the singlet oxygen generation drastically as compared to the substitutions at peripheral beta position. This is also evident from our results which clearly shows that upon irradiation, DPBF absorbance quenches within 25 seconds in case of α-ZnPc **(Figure 4 a-e)**. These results make both α-ZnPc and β-ZnPc to stand out as excellent photosensitizers to be employed for cancer therapy.

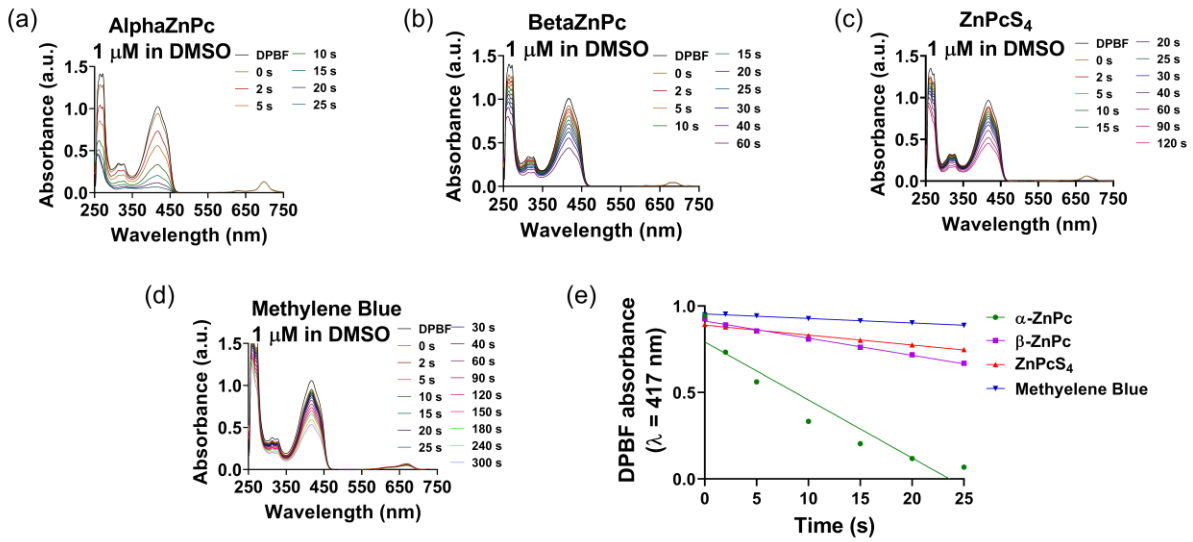

Figure 4: Changes in the absorption spectrum of DPBF upon irradiation in the presence of (a) α-ZnPc, (b) β-ZnPc, (c), $ZnPcS_4$, and (d) methylene blue; (e) Plot of absorbance of DPBF at 417 nm vs irradiation time in the presence of α-ZnPc, β-ZnPc, and $ZnPcS_4$ against methylene blue as the standard.

Rapid cellular uptake and exceptional intracellular ROS generation by agents upon irradiation

Cellular uptake of α-ZnPc and β-ZnPc in two pancreatic cancer cells, PANC-1 and BxPC-3, saturates within a short span of 4 hours as opposed to $ZnPcS_4$ which has an uptake of 60% and 10% in PANC-1 and BxPC-3, respectively **(Figure 5 a-d)**. The structural features of the proposed agents facilitate their rapid uptake within cancer cells which can potentially reduce the time gap between agent administration and therapy under the clinical settings.

$ZnPcS_4$ did not show any difference in the ROS levels without or with irradiation. Contrary to that, a basal level of intracellular ROS was detected without irradiation of the agents under the dark conditions. However, the intracellular ROS levels are significantly higher upon irradiation of α-ZnPc and β-ZnPc. The results show a remarkable cytotoxic potential of these agents towards cancer cells. Additionally, substitution at alpha position of isoindoline ring generates 2-fold higher intracellular ROS levels compared to the substitution at beta position upon 2-minutes of irradiation **(Figure 5 e,f)**. A secondary finding was a higher level of intracellular ROS in PANC-1 compared to BxPC-3 which might be attributed to the differences in the cell type, mechanism of which would be interesting to elucidate.

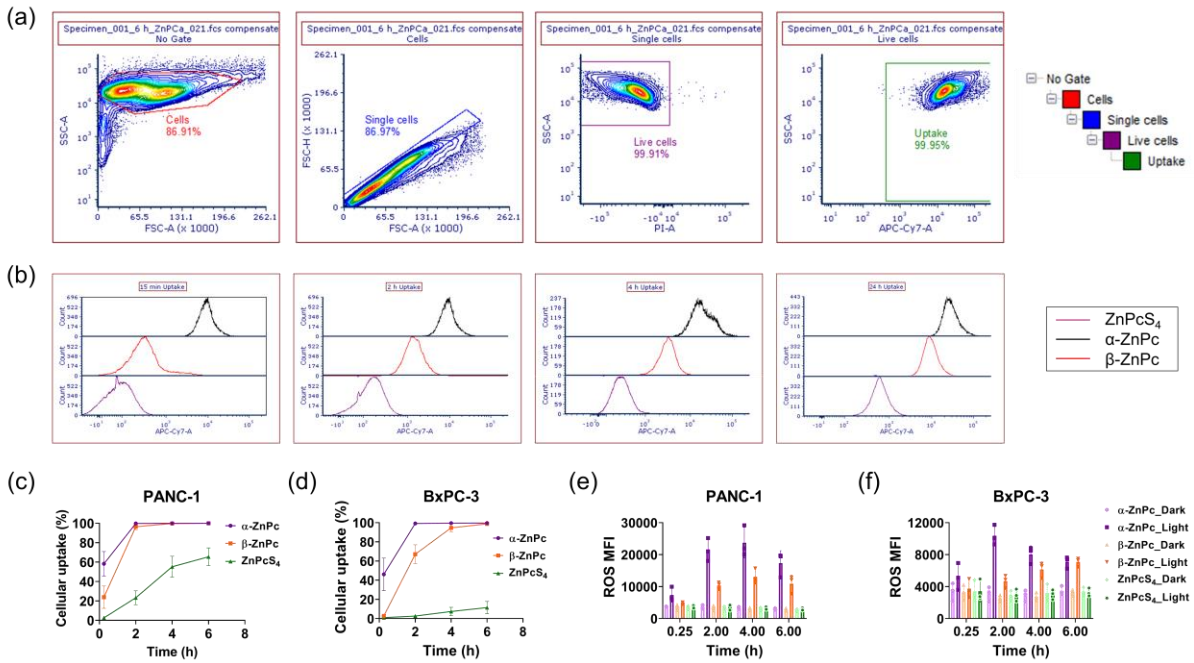

Figure 5: Cellular uptake and ROS generation through flow cytometer **(a)** Gating strategy used for quantifying cellular uptake; **(b)** Offset overlay depicting the cellular uptake of α-ZnPc, β-ZnPc, and $ZnPcS_4$ in 15 minutes, 2 hours, 4 hours and 24 hours; Cellular uptake of α-ZnPc, β-ZnPc, and $ZnPcS_4$ in **(c)** PANC-1 and **(d)** BxPC-3; ROS MFI with and without irradiation of α-ZnPc, β-ZnPc, and $ZnPcS_4$ in **(e)** PANC-1 and **(f)** BxPC-3.

Distinguished PDT potential of the agents *in vitro*

Both the proposed agents, α-ZnPc and β-ZnPc, did not show any cytotoxicity without laser irradiation commonly known as the dark cytotoxicity **(Figure 6 a,e,j,n)**. These agents are essentially photosensitizers and are supposed to generate cytotoxic species upon irradiation. When the agents were irradiated with a 740 nm lamp, 75% cytotoxicity was observed for α-ZnPc within 1-2 minutes of irradiation **(Figure 6 b,c,d,k,l,m)** and β-ZnPc at 10 minutes of irradiation **(Figure 6 f,g,h,o,p,q)**. The IC_{50} as low as 0.6-1.5 μM and 1.8-3.6 μM for α-ZnPc and β-ZnPc, respectively **(Figure 6 i,r)**. The cytotoxicity observed with α-ZnPc and β-ZnPc is unusually high within a minimal irradiation time relative to the photosensitizers reported in the literature, providing evidence for the phenomenal therapeutic potential of these agents.

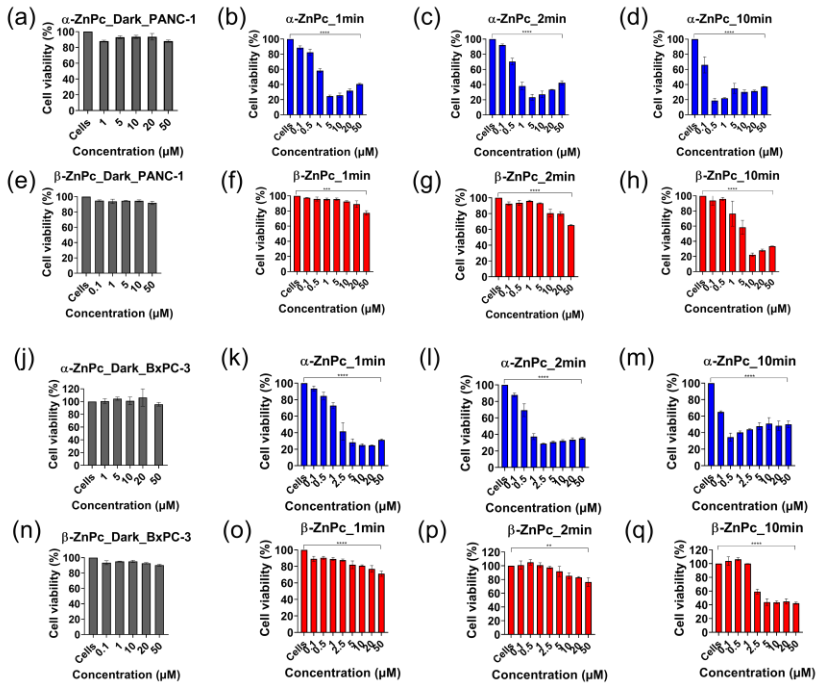

(i)

Agent (Irradiation time)	PANC-1 IC_{50} (μM)
α-ZnPc (1 min)	1.03
α-ZnPc (2 min)	0.60
α-ZnPc (10 min)	~0.07
β-ZnPc (1 min)	-
β-ZnPc (2 min)	22.59
β-ZnPc (10 min)	3.58

(r)

Agent (Irradiation time)	BxPC-3 IC_{50} (μM)
α-ZnPc (1 min)	1.43
α-ZnPc (2 min)	0.58
α-ZnPc (10 min)	-
β-ZnPc (1 min)	16.05
β-ZnPc (2 min)	8.41
β-ZnPc (10 min)	1.84

Figure 6: Dark cytotoxicity in **(a,e)** PANC-1 with α-ZnPc and β-ZnPc, **(j,n)** BxPC-3 with α-ZnPc and β-ZnPc; Light cytotoxicity with 1-minute irradiation in **(b,f)** PANC-1 with α-ZnPc and β-ZnPc ; Light cytotoxicity with 2-minute irradiation **(c,g)** PANC-1 with α-ZnPc and β-ZnPc,; Light cytotoxicity with 10-minute irradiation **(d,h)** PANC-1 with α-ZnPc and β-ZnPc, Light cytotoxicity with 1-minute irradiation in **(k,o)** BxPC-3 with α-ZnPc and β-ZnPc ; Light cytotoxicity with 2-minute irradiation **(l,p)** BxPC-3 with α-ZnPc and β-ZnPc,; Light cytotoxicity with 10-minute irradiation **(m,q)** BxPC-3 with α-ZnPc and β-ZnPc; IC_{50} for α-ZnPc and β-ZnPc with different irradiation times in **(i)** PANC-1 and **(r)** BxPC-3.

In vivo biodistribution and retention of the agent in tumor

Photoacoustic signal of α-ZnPc and β-ZnPc was detected at the tumor site within the first hour after injection, with peak accumulation at the 12-hour time point **(Figure 7 a-g)**, suggestive of a potential window for PDT illumination and subsequent monitoring via PA imaging. Therefore, the strong PA signals from α-ZnPc and β-ZnPc observed in the tumor region at the 12-hour time point suggests that PA imaging, combined with PDT, offers a novel theranostic approach with high translational potential.

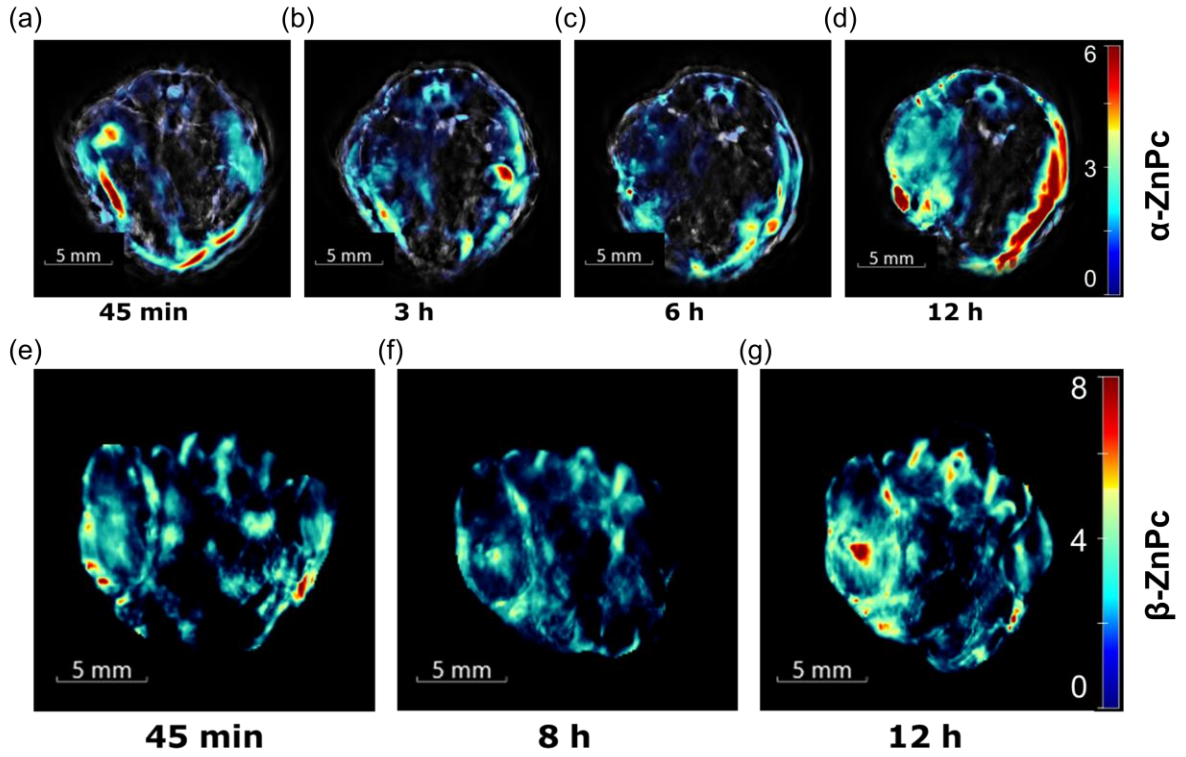

Figure 7: *In vivo* biodistribution of α-ZnPc at **(a)** 45 minutes **(b)** 3 hour **(c)** 6 hour **(d)** 12 hour and β-ZnPc at **(e)** 45 minutes **(f)** 8 hour **(g)** 12 hour

Agents cleared through hepatic and renal pathways post 24-h of tail vein injection

The *ex vivo* scans show that the PA signal intensity of agents drop at the tumor site post 24 hours of agent administration, indicating probe clearance within a day **(Figure 8 a-e)**. This allows for the longitudinal evaluation of PDT agent delivery after administration and can aid in optimizing PDT parameters and choosing of optimal dosing strategies. Apart from monitoring the retention in tumor, the biodistribution of agents was visualized and quantified in liver, kidney, spleen and heart, which facilitated the elucidation of clearance pathways. We hypothesize that α-ZnPc and β-ZnPc are cleared through both the hepatic and renal systems, because high concentrations of agents are found in the liver and kidneys **(Figure 8 f)**.

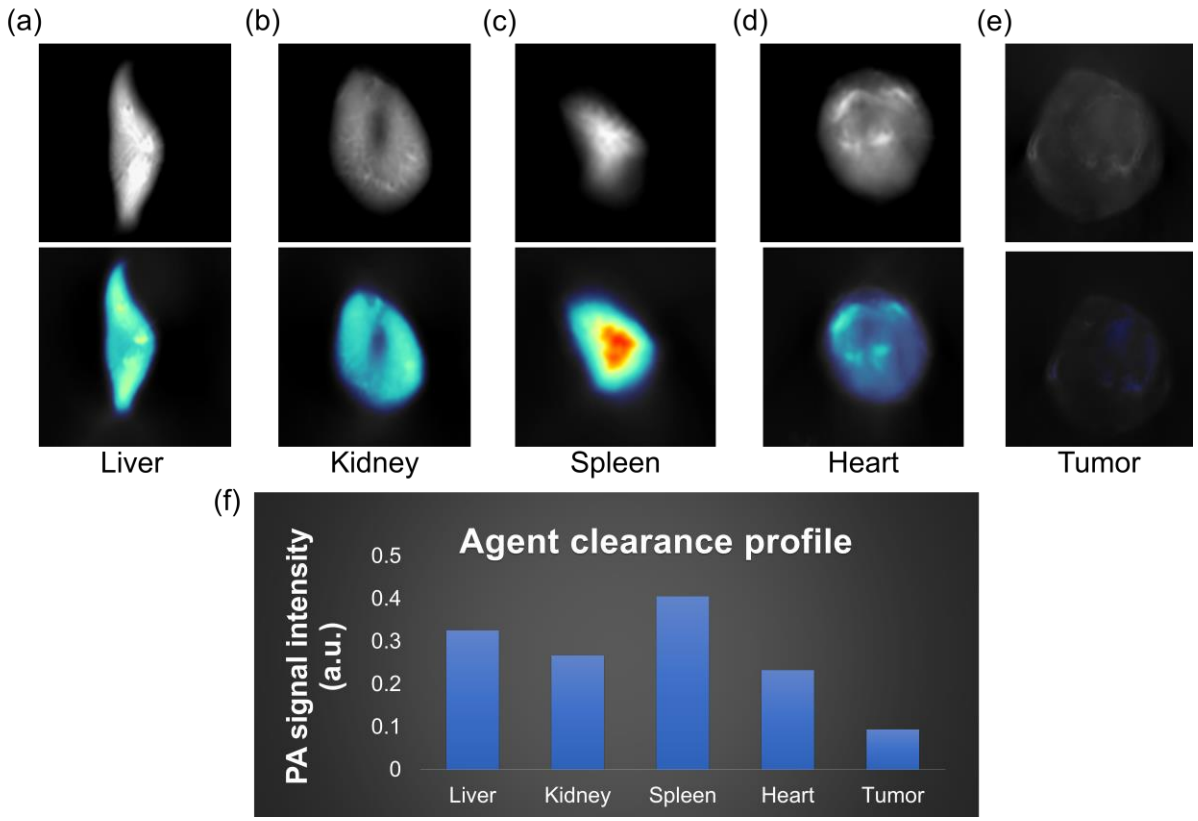

Figure 8: *Ex vivo* scans where top and bottom panels of **(a-e)** represents the respective anatomical images and accumulation of the agents in liver, kidney spleen, heart and tumor; **(f)** Agent clearance profile post 24 hours of agent administration.

Evaluation of the safety profiles of the agents

The hepatotoxicity and nephrotoxicity of anti-tumor drugs is a common adverse effect. H&E staining of the liver and kidney tissue was performed to evaluate the histopathological features (**Figure 9 a,b)**. After a single intravenous dose (200 μM, 200 μl) of α-ZnPc and β-ZnPc, no morphological or histopathological damage to the liver and kidney was observed indicating that 200 μM of the agents was not toxic to the liver and kidney.

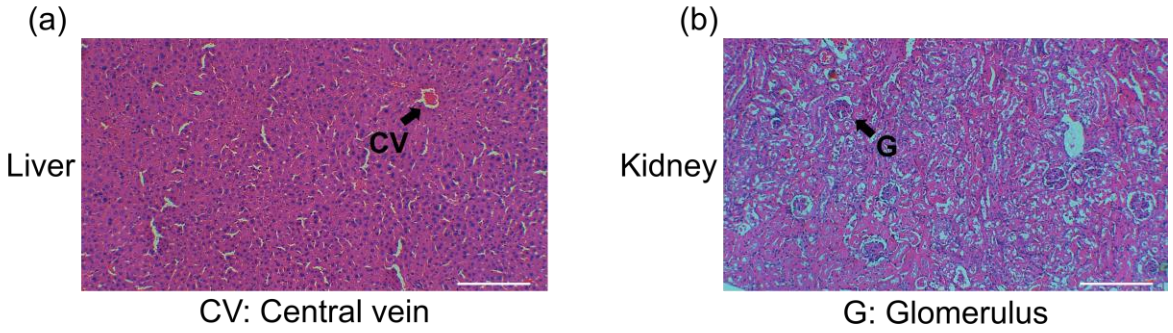

Figure 9: H&E staining of **(a)** liver and **(b)** kidney after agent administration. The scale bar denotes 100 μM.

STATISTICAL ANALYSIS

Statistical analysis was performed using Graphpad Prism. Quantitative data were expressed as mean ± s.e.m. A two-tailed Student's t-test was used to statistically compare the cell viability (%) between the control group (without agent addition) and the group of cells (BxPC-3 and PANC-1) treated with 50 μM concentration of α-ZnPc and β-ZnPc, with both groups irradiated for 1 minute, 2 minutes and 10 minutes. $P < 0.05$ was considered statistically significant.

DISCUSSION

The current study is motivated by the clinical need and impact of image guided therapy assessment for effective patient outcomes. The development of theranostic agents to meet this need has shown significant positive outcomes, although most theranostic agents in the clinic are nuclear medicine-based radiotracers. Our study focuses on a different imaging modality for diagnostics, namely photoacoustic imaging, one that does not involve radiation or radioactivity and combines both ultrasound and optical imaging into a single hybrid technique. In this study, we have demonstrated how photoacoustic imaging can be used to diagnose a tumor and plan for treatment, in this case photodynamic therapy with the same agent and further evaluate the efficacy of the treatment using the same photoacoustic contrast.

Previously, the photodynamic activity has been studied in tetrasubstituted $ZnPcS_4$ bearing, respectively, glycerol either in peripheral (4,5) or non-peripheral (3,6) positions of the isoindoline subunits.[13] The authors have reported that the ZnPc with glycerol substitution at peripheral (4,5) position did not show any LD_{90} value even at the highest concentration of 100 μM. However, ZnPc with non-peripheral (3,6) substitution gave an LD_{90} value of 35 μM. We have synthesized trisubstituted Pcs bearing substitutions at peripheral (4,5) or non-peripheral (3,6) positions of the isoindoline subunits showcasing IC_{50} as low as 0.6-1.5 μM within 1-2 minutes for non-peripheral substituition (α-ZnPc) and 1.8-3.6 μM in 10 minutes for peripheral substituition (β-ZnPc). A common -iodo substitution at one of the isoindoline subunits in both of our theranostic agents enhances the PDT efficacy by increasing the lifetime of triplet state of the PS.

In a study by Ho et al., ZnPc possessed the strongest PA signal with the highest relative PA quantum yield among the other tested compounds such as protoporphyrin IX, squaraine, chlorin e6 and methylene blue,[6] which highlights the reason for tailoring ZnPc scaffold to synthesize α-ZnPc and β-ZnPc in this study. We evaluated the tumor localization efficiency and biodistribution of the proposed agents longitudinally at different time points in a murine model using photoacoustic imaging. We observed a preferential tumor uptake of the agents as they localized in the tumor within 45 minutes post injection, reaching peak accumulation around 12 hours. The *ex vivo* scans acquired post 24 hours of agent administration implies probe clearance within a day. The future studies will aim at combining the PDT efficacy of α-ZnPc and β-ZnPc with their potential of photoacoustic imaging to achieve longitudinal monitoring of cancer progression and therapy *in vivo*.

IMPACT OF THE RESEARCH IN THE ADVANCEMENT OF KNOWLEDGE OR BENEFIT TO MANKIND

The current clinically validated theranostic agents belong to the class of radiopharmaceuticals and contain radioactive isotopes, such as, radioiodine for thyroid diseases. In contrast, our agents are based on zinc phthalocyanine scaffold which is devoid of any radioactivity, making them suitable for multiple disease-status monitoring sessions.

In the field of theranostics, the state-of-the-art approaches mainly employ the nanoparticles for this purpose. Abundant literature depicts the use of nanoparticles based theranostic agents with different combinations of therapeutic (such as photodynamic and photothermal therapy) and diagnostic (fluorescence and photoacoustic imaging) which suggests that nanoparticles-based strategies have been well-explored. Contrary to that, small molecule based theranostic agents are yet to be investigated.

The novelty of this work lies in the fact that our theranostic agents are built on small molecule scaffolds which has not been reported in the state-of-the-art methods. These agents have been synthesized and tailored such that they exhibit the photoacoustic properties and photodynamic therapy potential, which is many folds higher that the existing agents.

We have designed, synthesized and compared the theranostic potential of two agents, incorporated with -OH rich moiety tri-substituted at the three rings of zinc phthalocyanine scaffold at alpha and beta positions respectively and a common -iodo substitution at the fourth ring of the scaffold. This position-based comparison of theranostic potential has not been reported in the existing literature.

None of the published studies have described the application of these molecules as theranostic agents with PDT/PAI as the combined therapeutic and imaging modalities.

Utility: The target population for our agents can be broadly categorized into 2 groups:

(1.) People who are at a higher risk of developing pancreatic cancer, such as the diabetic population and people with chronic pancreatitis.
(2.) People who have already been diagnosed with pancreatic cancer and require treatment approaches better than chemo or radiotherapy.

Our agents have the potential to serve as a theranostic agent for pancreatic cancer, which is one of the deadliest forms of human cancer.

LITERATURE REFERENCES

(1) Bai, J.-W.; Qiu, S.-Q.; Zhang, G.-J. Molecular and functional imaging in cancer-targeted therapy: Current applications and future directions. *Signal Transduction and Targeted Therapy* **2023**, *8* (1), 89.
(2) Yang, J.; Zhang, G.; Li, Q.; Liao, C.; Huang, L.; Ke, T.; Jiang, H.; Han, D. Photoacoustic imaging for the evaluation of early tumor response to antivascular treatment. *Quantitative Imaging in Medicine and Surgery* **2019**, *9* (2), 160.
(3) Wang, Z.; Yang, F.; Cheng, Z.; Zhang, W.; Xiong, K.; Yang, S. Photoacoustic-guided photothermal therapy by mapping of tumor microvasculature and nanoparticle. *Nanophotonics* **2021**, *10* (12), 3359-3368.
(4) Hester, S. C.; Kuriakose, M.; Nguyen, C. D.; Mallidi, S. Role of ultrasound and photoacoustic imaging in photodynamic therapy for cancer. *Photochemistry and Photobiology* **2020**, *96* (2), 260-279.
(5) Zhang, Y.; Lovell, J. F. Recent applications of phthalocyanines and naphthalocyanines for imaging and therapy. *Wiley Interdisciplinary Reviews: Nanomedicine and Nanobiotechnology* **2017**, *9* (1), e1420.
(6) Ho, C. J. H.; Balasundaram, G.; Driessen, W.; McLaren, R.; Wong, C. L.; Dinish, U.; Attia, A. B. E.; Ntziachristos, V.; Olivo, M. Multifunctional photosensitizer-based contrast agents for photoacoustic imaging. *Scientific reports* **2014**, *4* (1), 5342.
(7) Rohrbach, D. J.; Salem, H.; Aksahin, M.; Sunar, U. Photodynamic therapy-induced microvascular changes in a nonmelanoma skin cancer model assessed by photoacoustic microscopy and diffuse correlation spectroscopy. In *Photonics*, 2016; MDPI: Vol. 3, p 48.
(8) Xiang, L.; Xing, D.; Gu, H.; Yang, D.; Yang, S.; Zeng, L.; Chen, W. R. Real-time optoacoustic monitoring of vascular damage during photodynamic therapy treatment of tumor. *Journal of biomedical optics* **2007**, *12* (1), 014001-014001-014008.
(9) Baskaran, R.; Lee, J.; Yang, S.-G. Clinical development of photodynamic agents and therapeutic applications. *Biomaterials research* **2018**, *22* (1), 1-8.
(10) Mahmoudi, K.; Garvey, K.; Bouras, A.; Cramer, G.; Stepp, H.; Jesu Raj, J.; Bozec, D.; Busch, T.; Hadjipanayis, C. 5-aminolevulinic acid photodynamic therapy for the treatment of high-grade gliomas. *Journal of neuro-oncology* **2019**, *141*, 595-607.
(11) Zhao, Z.; Chan, P.-S.; Li, H.; Wong, K.-L.; Wong, R. N. S.; Mak, N.-K.; Zhang, J.; Tam, H.-L.; Wong, W.-Y.; Kwong, D. W. Highly selective mitochondria-targeting amphiphilic silicon (IV) phthalocyanines with axially ligated rhodamine B for photodynamic therapy. *Inorganic Chemistry* **2012**, *51* (2), 812-821.
(12) Avşar, G.; Sari, F. A.; Yuzer, A. C.; Soylu, H. M.; Er, O.; Ince, M.; Lambrecht, F. Y. Intracellular uptake and fluorescence imaging potential in tumor cell of zinc phthalocyanine. *International Journal of Pharmaceutics* **2016**, *505* (1-2), 369-375.
(13) Zorlu, Y.; Ermeydan, M. A.; Dumoulin, F.; Ahsen, V.; Savoie, H.; Boyle, R. W. Glycerol and galactose substituted zinc phthalocyanines. Synthesis and photodynamic activity. *Photochemical & Photobiological Sciences* **2009**, *8*, 312-318.

31 August 2024